JCTC Journal of Chemical Theory and Computation

ARTICLE

pubs.acs.org/JCTC

Wavelet Transform for Spectroscopic Analysis: Application to Diols in Water

Francesco Muniz-Miranda,[†] Marco Pagliai,[‡] Gianni Cardini,[*,†,‡] and Vincenzo Schettino[†,‡]

[†]European Laboratory for Non-Linear Spectroscopy (LENS), via Nello Carrara 1, 50019, Sesto Fiorentino (FI), Italy

[‡]Dipartimento di Chimica "Ugo Schiff", Università degli Studi di Firenze, via della Lastruccia 3, 50019, Sesto Fiorentino (FI), Italy

ABSTRACT: Wavelet transform has been used to correlate spectroscopic and structural properties from trajectories obtained by *ab initio* molecular dynamics simulations. This method has been applied to hydrogen bond dynamics of glycols in heavy water solutions, showing how the stretching frequency of the *intra*molecular O−H bond changes with the *inter*molecular hydrogen-bond distance. The resulting wavelet spectrograms have been interpreted according to H-bond strength and stability.

1. INTRODUCTION

Classical and *ab initio* molecular dynamics (MD) simulations are powerful tools used to study the structure and dynamics of condensed systems. In particular, the Car−Parrinello approach is well suited to analyze condensed systems with fairly strong intermolecular interactions, like hydrogen bonding. For these specific interactions, the vibrational density of states (VDOS) and the vibrational spectra are particularly significant probes of the structural and dynamic properties of the system. Fourier Transform (FT) is the most commonly used mathematical tool to extract spectral information from time-resolved signals and from trajectories of molecular dynamics simulations. However, there is additional information hidden in the MD trajectories that cannot be sorted out by this approach. In fact, FT extracts the frequency content of a time signal, but it is unable to localize the frequency of a signal in time. This information could be relevant in enlightening the dynamics of the system and in the deconvolution of the steady state spectroscopic response. The wavelet transform (WT) is another type of integral transform, which is able to perform both time-frequency and multiresolution analysis, and for this reason, its use in theoretical and computational chemistry is gradually increasing. In particular, it has been applied to electronic structure calculations[1−5] and to molecular dynamics[6−8] also to obtain time-dependent vibrational frequencies.[9,10]

In the present work, WT has been used to correlate vibrational frequencies of two molecular systems with other time-dependent structural properties. The simulated molecular systems are two glycols in heavy water solutions, which have been investigated by *ab initio* molecular dynamics, using the Car−Parrinello method,[11] to take into account polarization effects and charge transfer and correctly describe the hydrogen-bond interactions. Therefore, structural and dynamic properties of the diols have been analyzed from the trajectories of the simulations.

WT has been employed to improve the analysis of H-bond dynamics and its relation with spectroscopic properties. Since in molecular dynamics simulations it is always possible to associate to each simulation step a structural quantity, a distance−frequency correlation showing how the VDOS changes with a particular H-bond length has been obtained.

The glycols simulated in the present work are propane-1,3-diol (propanediol, PDO) and ethane-1,2-diol (ethylene glycol, EG), two homologous compounds of industrial interest that interact with the aqueous solvent mainly through *inter*molecular hydrogen bonds. PDO is a transparent, nontoxic liquid glycol that can be obtained by fermentation of sugars and can replace other glycols in formulations where petroleum-free ingredients are needed.[12] EG is the lower homologue of PDO and is mainly used as an antifreeze and a medium for convective heat transfer due to its low freezing point. For both PDO and EG, a deep knowledge of the hydrogen-bond interactions and of the solvation dynamics is needed to improve their use in industrial applications. These glycols are study cases of particular interest since they have two interaction sites with the water solvent, and the analysis of the hydrogen bond features is challenging because of the overlap of the solvent−solvent and solute−solvent contributions.

The structure of the paper is as follows. In section 2, details of the computational procedure are reported, and the essentials of the wavelet analysis are described together with the implementation carried out in the present work. In section 3, the structural and electronic properties obtained with the usual Fourier Transform analysis are described, and then, the time-frequency analysis and the structure-frequency correlation obtained by wavelet analysis are discussed. Section 4 contains some concluding remarks.

2. COMPUTATIONAL DETAILS

Ab initio molecular dynamics simulations have been performed for PDO and EG in water. These simulations have been carried out with the CPMD package[13] in the microcanonical ensemble (NVE) in conjunction with the BLYP[14,15] exchange and correlation functional, in cubic boxes with edges of 12.7005 Å (for PDO) and 12.6819 Å (for EG), with periodic boundary conditions. The samples in the two simulation boxes are made of

Received: November 2, 2010
Published: February 23, 2011

Table 1. Structural Parameters

ethane-1,2-diol[a]	Howard et al.[22]	BLYP[b]	B3LYP[b]	MP2[b]	CPMD[c]
$r(C-C)$	1.514	1.527	1.517	1.513	1.523
$r(C-O_1)$	1.433	1.454	1.434	1.431	1.457
$r(C-O_2)$	1.421	1.440	1.421	1.418	1.444
$r(O_1-H)$	0.961	0.971	0.961	0.961	0.974
$r(O_2-H)$	0.964	0.975	0.965	0.964	0.977
$r(O_1\cdots H)$	2.331	2.434	2.399	2.323	2.418
$\theta(O_1-C-C)$	106.1	106.7	106.8	106.2	106.8
$\theta(O_2-C-C)$	111.2	112.2	112.0	111.1	112.2
$\phi(H-O_1-C-C)$	−166.0	−164.8	−166.7	−164.0	−166.6
$\phi(H-O_2-C-C)$	−51.5	−54.9	−53.6	−51.9	−52.1
propane-1,3-diol[a]	**Kinneging et al.[23]**	**BLYP[b]**	**B3LYP[b]**	**MP2[b]**	**CPMD[c]**
$r(C_3-C_4)$	1.514	1.533	1.523	1.518	1.528
$r(C_4-C_5)$	1.514	1.543	1.532	1.527	1.539
$r(C_3-O_1)$	1.410	1.461	1.439	1.435	1.465
$r(C_5-O_2)$	1.410	1.441	1.422	1.420	1.445
$r(O_1-H)$	1.040	0.972	0.962	0.962	0.975
$r(O_2-H)$	0.980	0.977	0.967	0.965	0.979
$r(O_1\cdots H)$	1.753	2.051	2.034	2.000	2.052
$\theta(O_1-C_3-C_4)$	112.0	108.4	108.6	108.0	108.9
$\theta(O_2-C_5-C_4)$	108.0	113.4	113.4	113.0	114.0
$\theta(C_3-C_4-C_5)$	112.0	113.9	113.8	112.9	114.1
$\phi(H-O_1-C_3-C_4)$	180.0	173.9	175.6	173.2	172.3
$\phi(H-O_2-C_5-C_4)$	−46.0	−46.3	−46.7	−48.4	−41.4

[a] Bond lengths in Å, angles in degrees. [b] DFT and MP2 calculations have been performed with the GAMESS[19] suite of programs in conjunction with the 6-311++G(d,p) basis set. [c] CPMD geometry optimizations have been performed with the same parameters reported for the molecular dynamics simulations.

one solute molecule and 64 D_2O molecules (at the experimental density of deuterated water, ∼1.106 g cm^{-3}). Norm-conserving Martins−Troullier[16] pseudopotentials have been used along with Kleinman−Bylander[17] decomposition, and the plane waves expansions have been truncated at 85 Ry (this choice has been shown to be particularly effective in CPMD simulations[18]). In order to use a larger time step (δt of 5 au ∼ 0.12 fs), hydrogen atoms have been replaced by deuterium atoms. The fictitious electronic mass has been set at 700 au to allow for a good decoupling between electronic and nuclear degrees of freedom. The systems have been thermalized by scaling the atomic velocities for 2 ps in order to keep the temperature at the value of 300 ± 50 K, and the trajectories for both systems have been collected for ∼32 ps.

The data collected from the two simulations of the glycols have been compared with corresponding CPMD simulations in vacuum. The computational parameters used in vacuum simulations, such as cell parameters, energy cutoff, and time step, are the same as those in water simulations. To further check the accuracy in the reproduction of the structural parameters for the isolated diols with the computational approach adopted, geometry optimizations have been carried out with the GAMESS package[19] at the MP2 and density functional theory (DFT) levels of theory (using the BLYP[14,15] and B3LYP[15,20,21] exchange-correlation functionals) with the 6-311++G(d,p) basis set.

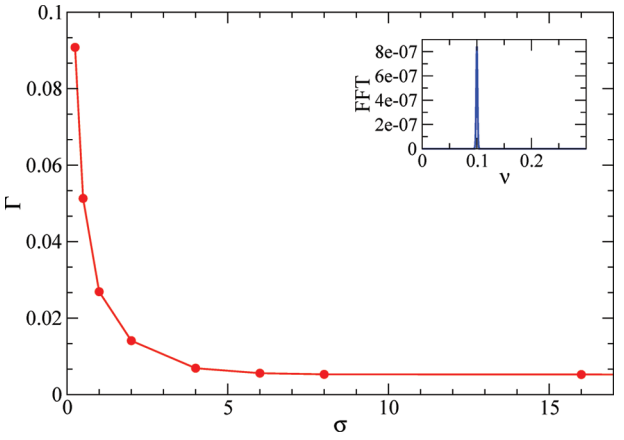

Figure 1. Spread of the wavelet spectrum of time signal in eq 8 as a function of the σ parameter (red). In the inset, the fast-Fourier transform (FFT) is reported as a blue line.

A comparison of experimental and calculated data is reported in Table 1, showing only minor differences between all electrons and pseudopotential calculations. All calculated normal mode frequencies are real and positive, ensuring that the systems are in their respective equilibrium configurations.

2.1. Wavelet Analysis. The FT is the conventional method used to extract the frequency content of a time-resolved signal $f(t)$:

$$\hat{f}(\omega) = \int_{-\infty}^{+\infty} dt\, e^{-i\omega \cdot t} f(t) \qquad (1)$$

A limitation of such an integral transform is that it cannot show how the frequency of interest changes with time due to variation of the intermolecular interactions.

Recently, it has been shown that WT can be applied to chemical problems,[24,25] and particularly to molecular dynamics simulations in order to sort out both structural and time-dependent properties.[6−10] Actually, WT can be seen as a mathematical tool that performs time-frequency analysis by using a set of time-window functions called wavelets, $\psi_{n,s}$, that sample the $f(t)$ signal. The $\psi_{n,s}$ wavelets are obtained by time-translation and time-dilatation of a generating function called "mother wavelet". These features are regulated by the couple of n and s integer parameters, as will be discussed in more detail in the following. In the present work, the Morlet-Gabor mother wavelet[26] has been used, which is a Gaussian-like function multiplied by a plane wave defined as

$$\psi(t) = \frac{1}{\pi^{1/4}} e^{i\omega_0 \cdot t}\, e^{-t^2/2\sigma^2} \qquad (2)$$

where ω_0 and σ represent the main oscillation frequency of the plane wave and the width at half-height of the Gaussian time-window, respectively. Kirby[27] showed that this mother wavelet is one of the most successful in reproducing the Fourier power spectra.

This function is translated and stretched by the n and s parameters, to give the entire set of wavelet functions $\{\psi_{n,s}\}$:

$$\psi_{n,s}(t') = \psi\left(\frac{t' - n \cdot t}{s}\right) \qquad (3)$$

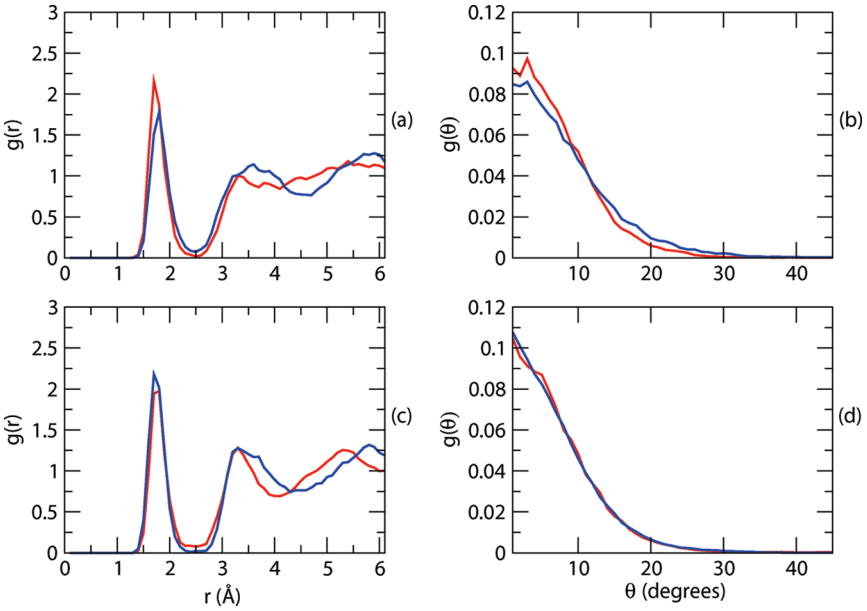

Figure 2. Acceptor $g(r)$ and $g(\theta)$: red for "site 1", blue for "site 2"; panels a and b for EG, panels c and d for PDO.

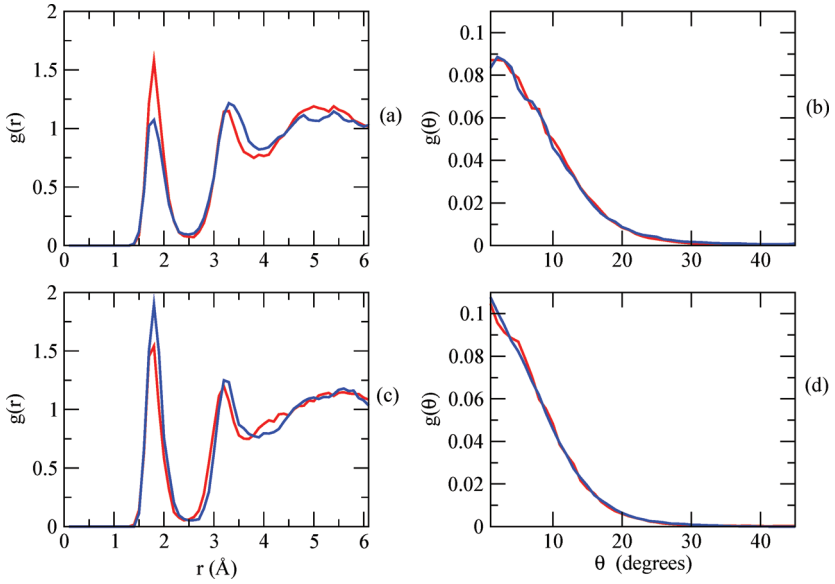

Figure 3. Donor $g(r)$ and $g(\theta)$: red for "site 1", blue for "site 2"; panels a and b for EG, panels c and d for PDO.

Table 2. Average Coordination Numbers

	site 1	site 2
EG donor	1.00	1.01
EG acceptor	1.70	1.42
PDO donor	0.98	1.00
PDO acceptor	1.56	1.94

The n parameter localizes the frequency in time, and $1/s$ is proportional to the frequency, whose detailed meaning will be illustrated in the following. The continuous WT is given by

$$\mathcal{W}(n,s) = \int_{-\infty}^{+\infty} \mathrm{d}t' f(t')\, \psi^*_{n,s}(t') \qquad (4)$$

while the discretized expression used in this work is[28]

$$\mathcal{W}(n,s) = \sum_{n'=0}^{N-1} f(n'\cdot\delta t)\, \psi^*\left[\frac{(n'-n)\cdot\delta t}{s}\right] \qquad (5)$$

In eq 5, the product $n'\delta t$ represents the total time at the n'th time-step of the molecular dynamics and localizes the signal in time. Thus, the wavelet transform $\mathcal{W}(n,s)$ gives the frequency content of the signal $f(t)$ over a Gaussian time-window centered at $n\delta t$. For the Morlet-Gabor set of basis functions,[28] the wavelength is defined as

$$\lambda = \frac{s4\pi}{\omega_0 + \sqrt{2+\omega_0^2}} \qquad (6)$$

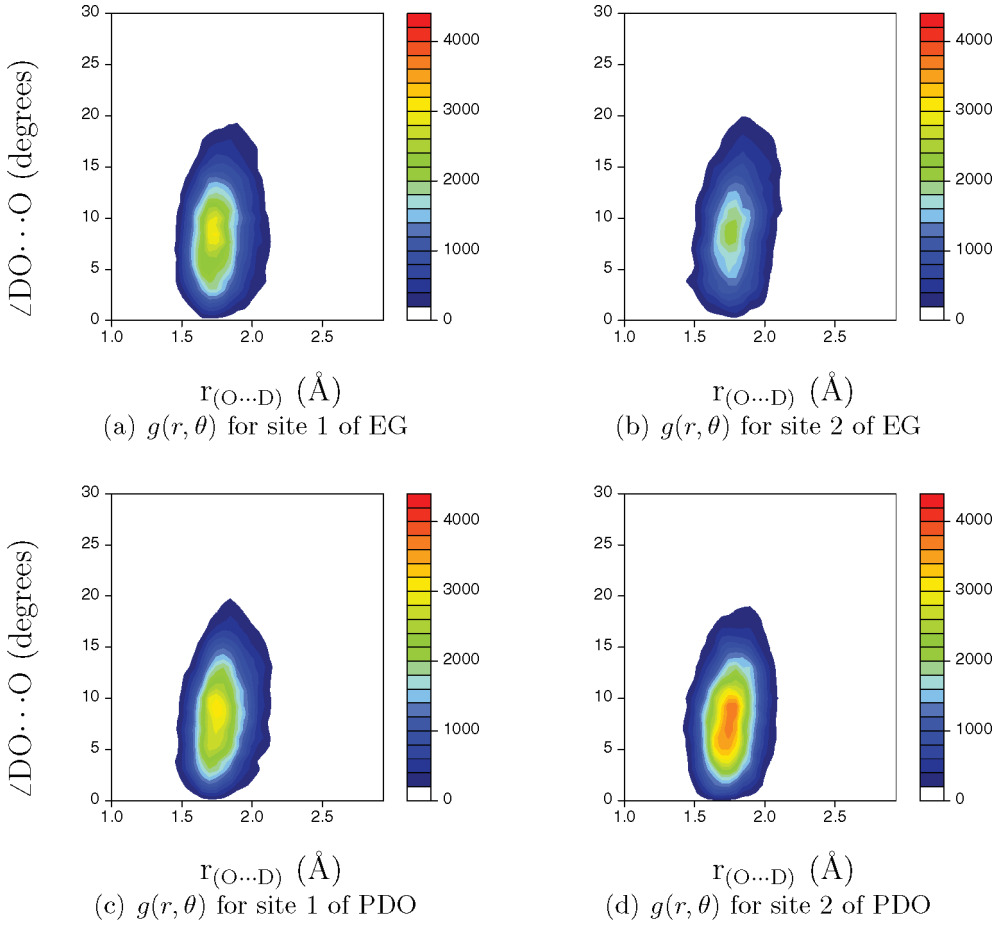

Figure 4. Weighted acceptor $g(r,\theta)$ for the two OD sites of the two diols.

while the corresponding effective frequency is proportional to $1/s$:

$$\nu = \frac{\omega_0 + \sqrt{2+\omega_0^2}}{s4\pi} \tag{7}$$

For $\omega_0 = 2\pi$ (as used in this work), the previous expression reduces to $\nu \simeq 1.01/s$. The parameter σ in eq 2 directly affects the time-frequency resolution, which is governed by a Heisenberg-like uncertainty principle.[29] In the present work, a value $\sigma = 2$ has been adopted in most spectrograms (unless otherwise specified) for a better time resolution. Similar choices for ω_0 (the main frequency) and σ parameters have been also adopted in refs 6 and 7. However, it must be pointed out that the choice of σ always represents a compromise between time and frequency resolution. This is shown in Figure 1 for a test function as

$$f_{\text{test}}(t) = \sin(kt + k')\, e^{-rt^2} \tag{8}$$

with k, k', and r real costants, whose fast-Fourier transform (FFT) is the Gaussian enlarged "Dirac's delta"-like function reported in blue in the inset of Figure 1. A roughly hyperbolic dependence of Γ (the width at half-height of the *frequency* peak of the test function) on σ is obtained, as shown in Figure 1.

When WT is used, it is possible to create a time-frequency plot. In the present work, where the main intermolecular interaction is the hydrogen bond between the solute diols and the solvent, we have analyzed both *intra-* and *inter*molecular structural properties. For the latter, defining the instantaneous bond length $r_{O\ldots D}(t)$ between the O atom of a water molecule and the D atom of the OD group of the solute, the time-resolved function $\Delta r_{O\ldots D}(t) = r_{O\ldots D}(t) - \langle r_{O\ldots D}(t)\rangle$ has been taken as the fluctuation of the H-bond length. In the same manner, $\Delta r_{O-D}(t)$ is the fluctuation of the *intra*molecular O−D bond length of the diols. Equation 5, in these cases, produces a wavelet spectrogram that displays the change in time of the VDOS of the H-bond and O−D stretching mode, respectively.

The algorithm implemented in the present work looks for the value that maximizes the modulus $|\mathcal{W}(n,s)|^2$ of the WT at a given time step n'. The corresponding value of $1/s$ is taken as the "instantaneous stretching frequency". The same approach has been used to analyze *intra*molecular features by adopting as the input function the O−D bond length fluctuation of the hydroxyl groups of the glycols. The computer program developed in this work calculates the WT directly. A cutoff of $\pm 3\sigma$ from the maximum of the Gaussian Gabor-Morlet wavelet function has been used to allow the retention of more than 99.7% of the power spectrum energy and to save computation time.

3. RESULTS AND DISCUSSION

3.1. Structural and Electronic Properties. *3.1.1. Structural Properties.* PDO and EG interact with water mainly through H bonds, acting as both an acceptor and a donor. The hydrogen bond can be characterized structurally through the O−D···O distance r and the O−D···O angle θ. Figures 2 and 3 report the pair radial $g(r)$ and angular $g(\theta)$ distribution functions for the acceptor and donor H-bonds, respectively. It can be seen that

dx.doi.org/10.1021/ct100625e |J. Chem. Theory Comput. 2011, 7, 1109–1118

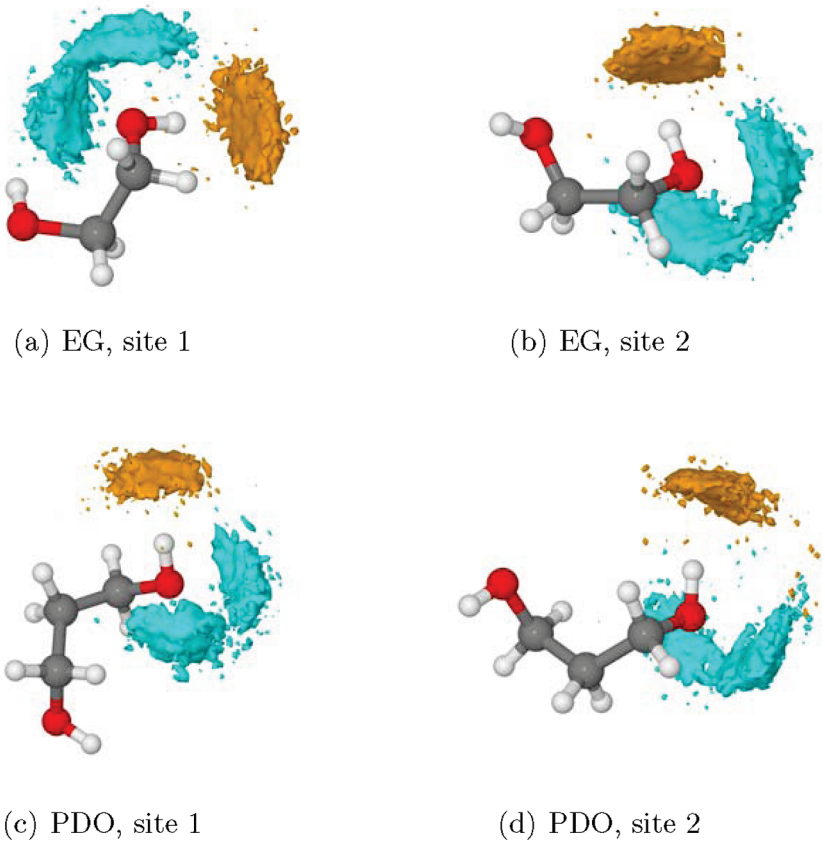

Figure 5. SDF of PDO and EG. Cyan and orange surfaces show the mobility of D and O atoms of H-bonded water molecules, respectively.

radial distribution functions of the two glycols differ very slightly. The deep first minima are indicative of the slow mobility of the water molecules bound to the glycols. On the contrary, it can be noted that the $g(\theta)$ functions for PDO are narrower, probably due to the fact that the two OD sites are farther away than in EG, allowing more independent solvation dynamics. This also implies that the angular parameters can be more sensitive to structural details. In the present case, the narrower $g(\theta)$ function is evidence for a more stable H-bond in the PDO solution.

The average coordination number for the OD sites, extracted from $g(r)$, is reported in Table 2 and is always close to the expected value of 1 for the donor interactions, whereas the acceptor coordination number is larger and shows a significant spread as a consequence of weaker interactions. The differences occurring for sites 1 and 2 of both diols arise from statistical uncertainty due to the finite temporal length of the simulations and the use of a single solute molecule for each system.

To better characterize the strength and structural features of the hydrogen bond, the weighted joint radial and angular distribution function $g(r,\theta)$ can be calculated by adopting the weighting function F_{HB}:[30−32]

$$F_{HB} = A(r(t)) \times B(\theta(t)) \tag{9}$$

$$A(r(t)) = \begin{cases} \exp(-(r_e - r(t))^2/2\sigma_r^2) & \text{if } (r_e - r(t)) < 0 \\ 1 & \text{if } (r_e - r(t)) \geq 0 \end{cases} \tag{10}$$

Table 3. Average Dipole Moments for Diols According to MLWF Center Analysis on the Three Model Systems

	isolated diol	diol + H-bonded water molecules	diol in solution
EG	2.71 D	3.11 D	4.55 D
PDO	2.05 D	2.18 D	3.87 D

$$B(\theta(t)) = \begin{cases} \exp(-(\theta_e - \theta(t))^2/2\sigma_\theta^2) & \text{if } (q_e - q(t)) < 0 \\ 1 & \text{if } (q_e - q(t)) \geq 0 \end{cases} \tag{11}$$

$$g(r,\theta) = h(r) \times h(\theta) F_{HB} \tag{12}$$

The values of the r_e, θ_e, σ_r, and σ_θ parameters are extrapolated from unnormalized pair radial and angular distribution functions $h(r)$ and $h(\theta)$: r_e is the distance associated with the first local maximum in $h(r)$, and θ_e is the angle associated with the first local maximum of $h(\theta)$. σ_r and σ_θ are the half-widths at half-height in $h(r)$ and $h(\theta)$, respectively.

The results shown in Figure 4 confirm that H-bonding in PDO is stronger, due to the lower spread of the joint distribution function along the angular parameters, since in the present simulations the angular conditions are a more stringent requirement for the hydrogen bond formation. A pictorial view related to the weighted $g(r,\theta)$ is shown in Figure 5, where the spatial distribution functions (SDF) of the OD groups of the water molecules are reported, displaying a three-dimensional description

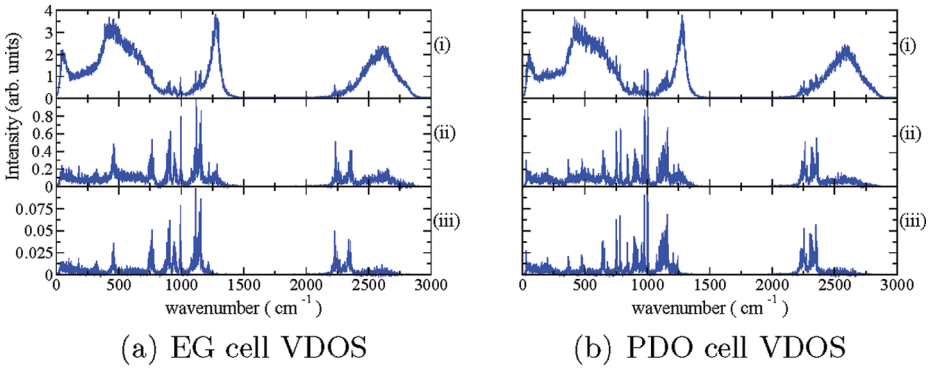

Figure 6. Vibrational densities of states: (i) VDOS of the complete simulation cells, (ii) VDOS of the diols and the two H-bonded water molecules, (iii) VDOS of the diols by themselves.

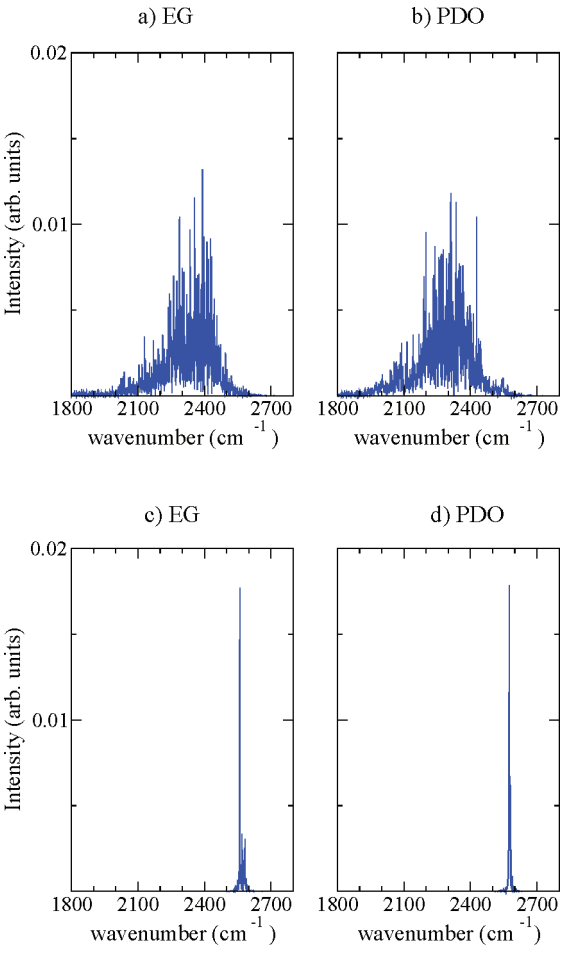

Figure 7. VDOS for hydroxyl group stretching mode in water (panels a and b) and in vacuum (panels c and d) simulations.

of the motion for the water molecules around the OD groups of the diols.

The cyan-colored isosurfaces (each point has been visited at least 55 times) close to the glycols represent the probability to find the D atoms of water around the O sites of the solutes, whereas the orange-colored ones represent the probability to find the O atoms of water around the alcoholic D atoms of the diols. These combined isosurfaces give a clear representation of the global mobility of the solvation cage. The spread of the

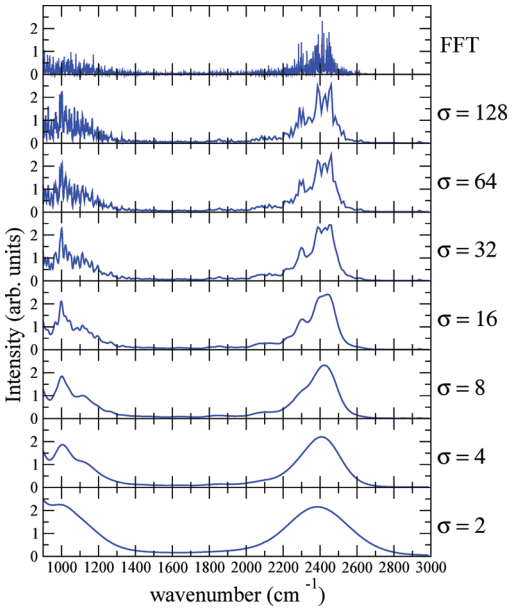

Figure 8. Fourier and wavelet power spectrum of the displacement of *inter*molecular $\Delta r_{O\ldots D}(t)$ function of EG, site 2.

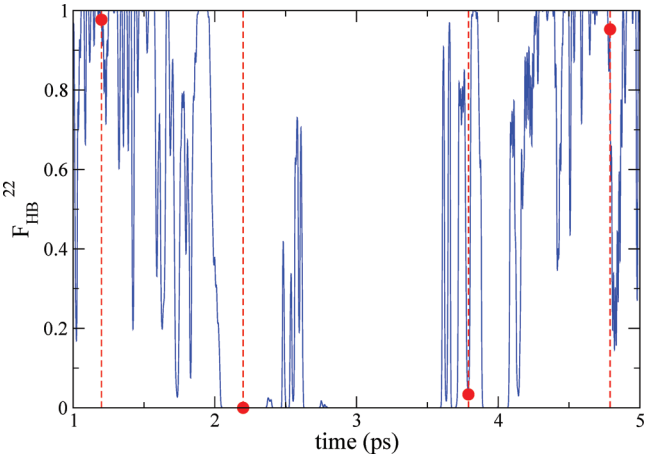

Figure 9. F_{HB} evolution with time for the interaction of D_2O molecule #22 with site 1 of PDO (full blue line). In dotted red lines are the sampled time steps for which the wavelet spectra are reported in Figure 10. The red circles represent the F_{HB}^{22} value sampled at those time steps.

isosurfaces for PDO is smaller than for EG, in line with the previous observations from the $g(\theta)$ and $g(r,\theta)$ functions.

3.1.2. Electronic Structure Analysis. The polarization effects due to the interaction of the glycols with the solvent have been analyzed in terms of Maximally Localized Wannier Functions (MLWF) centers.[33,34] The positions of the MLWF centers can be related to the electron pairs and give a direct picture of the electronic structure. In order to obtain useful insight on the electronic structure changes due to the interactions of the glycols with the solvent, the molecular dipole moment computed on the basis of the MLWF centers positions of PDO and EG has been monitored during the simulations. For this purpose, the dipole moments of PDO and EG have been calculated on a series of time-equispaced configurations obtained by CPMD simulations (1 configuration every 10^4 time-steps, corresponding to 1.2 ps). The polarization enhancement of glycols in solution has been obtained by adopting the following computational strategy. For each configuration, the MLWF centers have been obtained for all of the system, for the diols and the H-bonded water molecules and for diols alone without geometry optimization.

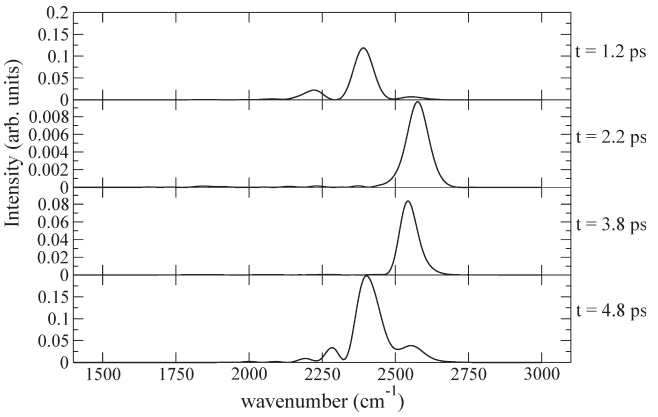

Figure 10. Wavelet spectra at four different time-steps calculated from the *intra*molecular $\Delta r_{O-D}(t)$ function for site 1 of PDO (parameter $\sigma = 10$).

In Table 3, the dipole moments calculated by MLWF center analysis by localizing the valence shell electron doublets are reported. The dipole moment of the diols increases as reported in Table 3, as a consequence of the interaction with the solvent. The time dependent data also show an evident correlation in the time evolution of the dipole moments for the three model systems. However, the solvent increases the dipole moment of the diols, and larger fluctuations are observed for EG, which being smaller in size is more sensitive to polarization effects by the water cage. Furthermore, the dipole moment increase, due to solvent interaction, is larger in EG than in PDO for the same reason.

3.2. Time-Frequency Analysis. In Figure 6, the VDOS of the water solutions, of the diols with the two closest molecules, and of the diols by themselves in the water solutions are shown, obtained by FFT of the velocity autocorrelation functions. The OD stretching region (2100−2600 cm^{-1}), which is the most interesting region of the spectrum, will be discussed in the following on the basis of WT analysis.

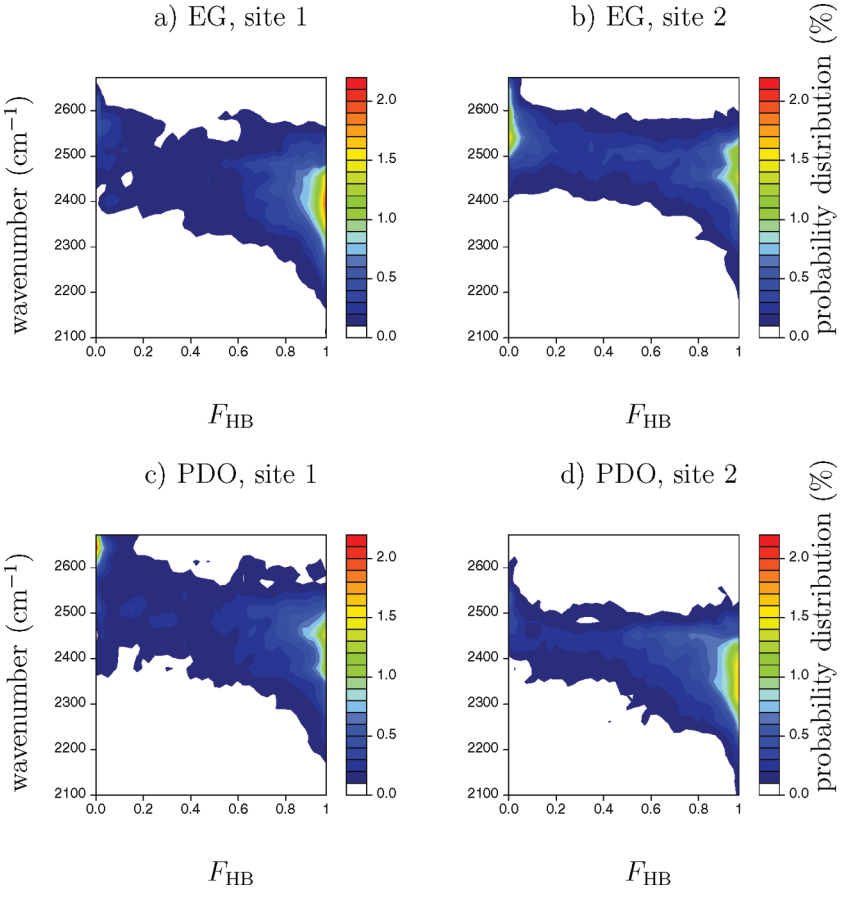

Figure 11. Correlation spectrograms between O−D stretching frequency and F_{HB} function.

dx.doi.org/10.1021/ct100625e |*J. Chem. Theory Comput.* 2011, 7, 1109–1118

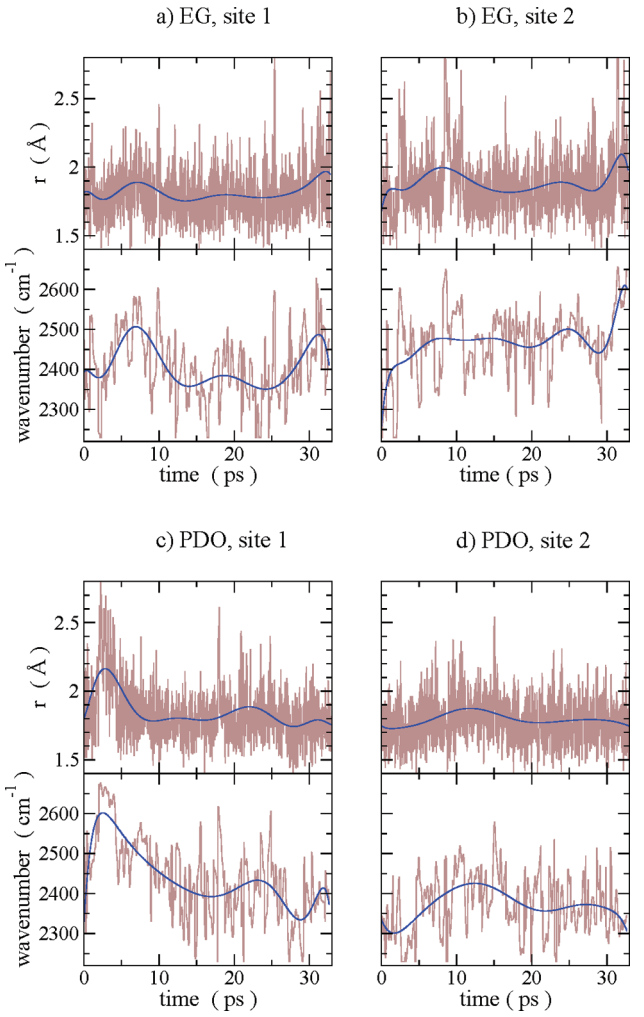

Figure 12. Comparison of the time evolutions of H-bond length and O−D stretching frequency. The brown lines correspond to the actual values found during the simulations, whereas the blue lines represent the smoothed trends of the former.

The structure of the OD stretching band results from the convolution of solvent−solvent and solute−solvent interactions, and we focus on the structure, extracted from the simulation, of the VDOS of the solute molecule and of the two nearest water molecules bound to the diols. This can be appreciated in more detail when analyzing the VDOS extracted by FFT of the oscillations of the intramolecular Δr_{O-D} functions, as reported in Figure 7, where the density of states obtained by simulations of the diols in solution (panel *a* and *b*) and in a vacuum (panel *c* and *b*) are reported. The red shift due to H-bonding interactions with the water solvent is evident, along with the broadening of the stretching band.

In Figure 8, the FFT of this feature of the simulation cell is compared with the WT at various values of the σ parameter showing details of the band structure at increasing resolution, using the *inter*molecular $\Delta r_{O\cdots D}(t)$ fluctuation as an input function.

The WT appears to correctly reconstruct the Fourier spectrum with high values of parameter σ, showing that the truncation in the Gabor-Morlet wavelet does not significantly affect the calculations. The inhomogeneous broadening of the band can be attributed to time changes of the structure of the solvent cage around the hydroxyl groups of the diols, which modulates the instantaneous vibrational frequency.

To better enlighten the origin of the various frequency components, the trajectory of site 1 of PDO has been analyzed by WT at specific time intervals. Figure 9 shows the details of the trajectory referring to site 1 of PDO. It can be seen that along the first 5 ps of simulation, site 1 is alternatively free or bound to water molecule #22. Later, along the trajectory, the site is constantly bound to the same water molecule.

The wavelet transform spectrum has been calculated at the simulation times of 1.2, 2.2, 3.8, and 4.8 ps (dotted red lines in Figure 9), and the results, reported in Figure 10, clearly show that the red shift nicely correlates with the H-bonding character. The same correlation has been observed at all time-steps probed for both sites of the two glycols.

An alternative and more immediate way of illustrating this behavior is obtained by directly correlating the most intense O−D stretching frequency, obtained by WT of the corresponding $\Delta r_{O-D}(t)$ function, with the values of the F_{HB} donor function. This is displayed in Figure 11 showing how the wavelet-calculated VDOS for all OD sites of the diols changes with the value of the F_{HB} function (which is confined in the [0−1] interval due to the fact that only a single donor H-bond can be present at a time). The plotted quantities are the probability distributions of the VDOS, which thicken and are red-shifted when F_{HB} approaches 1, meaning that the *inter*molecular H-bond lowers the O−D *intra*molecular stretching frequency. Consistently, the VDOS is peaked at higher frequencies when $F_{HB} \simeq 0$. As can be seen, there is a sort of pathway between the two extremes in the frequency/configurational space explored by the simulations. For site 2 of both glycols, the pathway is continuous, due to the more oscillating character of the F_{HB} function with oscillations too fast to be precisely resolved even with WT.

As a whole, the present analysis shows how a structural quantity like F_{HB}, designed as a probe of the H-bonding, can be efficiently correlated with the stretching frequency of an *intra*molecular vibration, because the molecular oscillators are coupled to the water environment and are sensitive to small fluctuations in the solvation cage. Moreover, the advantage of a continuous function like F_{HB} to monitor on the fly the dynamics of the hydrogen bond and its effect on the vibrational spectrum is quite evident.

Wavelet analysis has also been used to sort out the time evolution of the frequency related to the most intense peak in the high resolution spectra (obtained like those of Figure 10) and its correlation with the *inter*molecular O···D bond length between nearest molecules along the simulation. The result is shown in Figure 12. The blue line in Figure 12, drawn as a guide for the eye, has been obtained by a 10th-order polynomial fit of the raw data.

A straight correlation between the time evolution of vibrational frequencies and the time evolution of *intra*molecular O−D stretching distance can be appreciated.

A more straightforward way to show the correlation between stretching frequencies and *inter*molecular $D_{diol}\cdots O_{water}$ distance is via the bidimensional spectrogram plot of Figure 13, where distance and frequency are directly correlated at each time step. The probability distribution reported in Figure 13 represents the maximum of the *intra*molecular O−D band stretching obtained by WT correlated with the corresponding value of the *inter*molecular H-bond length.

These spectrograms show the same "*banana shaped*" distributions (as referred to in refs 6 and 7) obtained for other systems like heavy water and Cl^- anions in heavy water. Moreover, the same type of shape is obtained using *inter*molecular H-bond distances or *intra*molecular O−D bond lengths, since they both

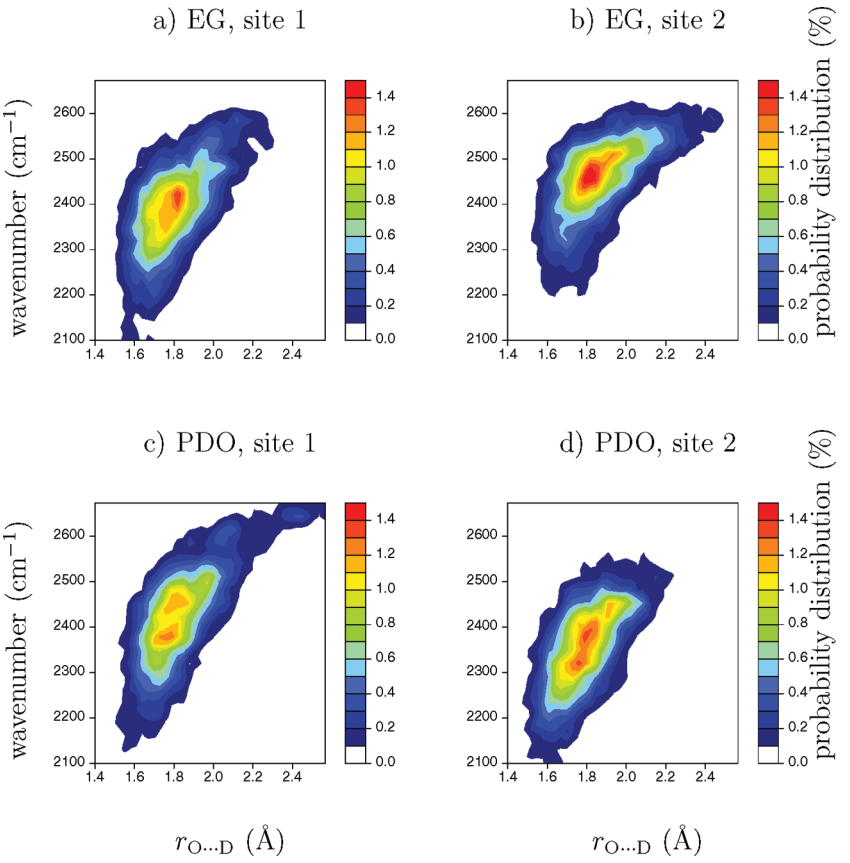

Figure 13. H-bond length−frequency spectrograms for both PDO and EG.

mainly probe the stretching frequency associated with the O−D stretching of the glycols. The VDOS thickens at bond lengths corresponding to the first peak of the $g(r)$ and $g(r,\theta)$ functions. The frequency shift is thus simply correlated to the strength and stability of the H-bond. A strong H-bond gives a $g(r)$ function peaked at shorter distances, and within the harmonic approximation, it reduces the intramolecular stretching force constant and, consequently, shifts the VDOS at smaller wavenumbers. The slightly different plot for EG, site 2, is due to the fact that the most strongly interacting water molecule for that site is not H-bonded for the first picosecond of simulation, thus resulting in a final spectrogram showing a weaker H-bond, as expected.

It is not possible to establish an exact bijective relationship between bond length and frequency, but this is not surprising because the radial distance is only one of the structural parameters that characterize the H-bond, the other being the angular parameter. Hence, the distance is degenerate in the angle space. Moreover, the Heisenberg-like uncertainty principle between time and frequency, and therefore between distance and frequency, affects the spectrogram resolution. However, these plots clearly show that a reliable correlation between bond length and density of vibrational states exists, which can be understood on the basis of the H-bond stability. This is in agreement with previous results obtained using static *ab initio* calculations.[35]

4. CONCLUSIONS

In the present work, the hydrogen bond structure and dynamics of two prototype glycols, ethylene glycol and propanediol, in water solutions have been studied by *ab initio* molecular dynamics simulations in the density functional theory approach. Molecular dynamics trajectories have been obtained using the Car−Parrinello (CPMD) method and have been analyzed by both the traditional Fourier transform and the wavelet transform methods. It has been shown that a good deal of novel information can be obtained by the time analysis supplied by the wavelet analysis. In particular, it has been found that the complex pattern of the hydrogen bond stretching mode has an inhomogeneous origin and arises from the convolution of a number of differently shifted vibrational modes that can be sorted out by wavelet transform at different time intervals of the molecular dynamics simulation. The time-resolved vibrational modes obtained by the wavelet analysis can be correlated in a straightforward way with the structure of the solvent cage around the solute diols and with structural parameters like the O−D bond length or with the strength of the hydrogen bonding. A careful comparison of the Fourier and wavelet transforms also shows that for a more accurate characterization of the hydrogen bonding a simultaneous consideration of the bond length (e.g., $r_{O-D\cdots O}$) and of the $\angle$O−D···O angle is needed. The wavelet transform analysis is not only a suitable tool to analyze the vibrational features in terms of modulation of the local structure of the solvation cage but also offers unique opportunities to study time-resolved spectroscopic experiments.

AUTHOR INFORMATION

Corresponding Author

*E-mail: gianni.cardini@unifi.it.

■ ACKNOWLEDGMENT

This work was supported by the Ministero dell'Istruzione, dell'Università e della Ricerca (MIUR). The authors would like to thank the CINECA Supercomputing Center for the allocation of computing resources and Prof. Roberto Righini (LENS) for useful discussions.

■ REFERENCES

(1) Goedecker, S.; Ivanov, O. V. *Phys. Rev. B* **1999**, *59*, 7270–7273.
(2) Neelov, A. I.; Goedecker, S. *J. Comput. Phys.* **2006**, *217*, 312–339.
(3) Daykov, I. P.; Arias, T. A.; Engeness, T. D. *Phys. Rev. Lett.* **2003**, *90*, 216402–216405.
(4) Engeness, T. D.; Arias, T. A. *Phys. Rev. B* **2002**, *65*, 165106–165115.
(5) Cho, K.; Arias, T. A.; Joannopoulos, J. D.; Lam, P. K. *Phys. Rev. Lett.* **1993**, *71*, 1808–1811.
(6) Mallik, B. S.; Semparithi, A.; Chandra, A. *J. Chem. Phys.* **2008**, *129*, 194512–194527.
(7) Mallik, B. S.; Semparithi, A.; Chandra, A. *J. Phys. Chem. A* **2008**, *112*, 5104–5112.
(8) Askar, A.; Cetin, A. E.; Rabitz, H. *J. Phys. Chem.* **1996**, *100*, 19165–19173.
(9) Rahaman, A.; Wheeler, R. A. *J. Chem. Theory Comput.* **2005**, *1*, 769–771.
(10) Pagliai, M.; Muniz-Miranda, F.; Cardini, G.; Righini, R.; Schettino, V. *J. Phys. Chem. Lett.* **2010**, *1*, 2951–2955.
(11) Car, R.; Parrinello, M. *Phys. Rev. Lett.* **1985**, *55*, 2471–2474.
(12) Orts, W. J.; Holtman, K. M.; Seiber, J. N. *J. Agric. Food Chem.* **2008**, *56*, 3892–3899.
(13) *CPMD*; MPI für Festkörperforschung Stuttgart: Stuttgart, Germany, 1997−2001; IBM Corp.: Armonk, New York, 1990−2008.
(14) Becke, A. D. *Phys. Rev. A* **1988**, *38*, 3098–3100.
(15) Lee, C.; Yang, W.; Parr, R. G. *Phys. Rev. B* **1988**, *37*, 785–789.
(16) Troullier, N.; Martins, J. L. *Phys. Rev. B* **1991**, *43*, 1993–2006.
(17) Kleinman, L.; Bylander, D. M. *Phys. Rev. Lett.* **1982**, *48*, 1425–1428.
(18) Kuo, I. F. W.; Mundy, C. J.; McGrath, M. J.; Siepmann, J. I.; VandeVondele, J.; Sprik, M.; Hutter, J.; Chen, B.; Klein, M. L.; Mohamed, F.; Krack, M.; Parrinello, M. *J. Phys. Chem. B* **2004**, *108*, 12990–12998.
(19) Schmidt, M. W.; Baldridge, K. K.; Boatz, J. A.; Elbert, S. T.; Gordon, M. S.; Jensen, J. H.; Koseki, S.; Matsunaga, N.; Nguyen, K. A.; Su, S. J.; Windus, T. L.; Dupuis, M.; Montgomery, J. A. *J. Comput. Chem.* **1993**, *14*, 1347–1363.
(20) Becke, A. D. *J. Chem. Phys.* **1993**, *98*, 5648–5652.
(21) Becke, A. D. *J. Chem. Phys.* **1993**, *98*, 1372–1377.
(22) Howard, D.; Jorgensen, P.; Kjaergaard, H. G. *J. Am. Chem. Soc.* **2005**, *127*, 17096–17103.
(23) Kinneging, A.; Mom, V.; Mijlhoff, F. C.; Renes, G. H. *J. Mol. Struct.* **1982**, *82*, 271–275.
(24) Shao, X. G.; Leung, A. K. M.; Chau, F. T. *Acc. Chem. Res.* **2003**, *36*, 276–283.
(25) Ehrentreich, F. *Anal. Bioanal. Chem.* **2002**, *372*, 115–121.
(26) Carmona, R.; Hwang, W.; Torresani, B. *Practical Time-Frequency Analysis: Gabor and Wavelet Transforms with an implementation*; Academic Press: New York, 1998.
(27) Kirby, J. F. *Comput. Geosci.* **2005**, *31*, 846–864.
(28) Torrence, C.; Compo, G. P. *Bull. Am. Meteorol. Soc.* **1998**, *79*, 61–78.
(29) Chui, C. K. *An introduction to wavelet; Wavelet analysis and its applications*; Academic Press, Inc.: New York, 1992.
(30) Pagliai, M.; Cardini, G.; Righini, R.; Schettino, V. *J. Chem. Phys.* **2003**, *119*, 6655–6662.
(31) Pagliai, M.; Cardini, G.; Schettino, V. *J. Phys. Chem. B* **2005**, *109*, 14923–14928.
(32) Faralli, C.; Pagliai, M.; Cardini, G.; Schettino, V. *J. Phys. Chem. B* **2006**, *110*, 14923–14928.
(33) Marzari, N.; Vanderbilt, D. *Phys. Rev. B* **1997**, *56*, 12847–12862.
(34) Silvestrelli, P. L.; Marzari, N.; Vanderbilt, D.; Parrinello, M. *Solid State Commun.* **1998**, *107*, 7–11.
(35) Klein, R. A. *J. Comput. Chem.* **2002**, *23*, 585–599.